Supporting Information for:

Phytochemicals perturb membranes and promiscuously alter protein function

Helgi I. Ingólfsson[1,2,*], Pratima Thakur[3], Karl F. Herold[4], E. Ashley Hobart[5], Nicole B. Ramsey[5], Xavier Periole[2], Djurre H. de Jong[1,2], Martijn Zwama[2], Duygu Yilmaz[2], Katherine Hall[6], Thorsten Maretzky[6], Hugh C. Hemmings Jr.[4], Carl Blobel[6], Siewert J. Marrink[1,2], Armağan Koçer[2], Jon T. Sack[3,*], Olaf S. Andersen[5,*]

[1]Zernike Institute for Advanced Materials, University of Groningen, Groningen, The Netherlands
[2]Groningen Biomolecular Science and Biotechnology Institute, University of Groningen, Groningen, The Netherlands
[3]Dept. Physiology and Membrane Biology, University of California, Davis, CA, USA
[4]Dept. Anesthesiology, Weill Cornell Medical College, New York, NY, USA
[5]Dept. Physiology and Biophysics, Weill Cornell Medical College, New York, NY, USA
[6]Hospital for Special Surgery, New York, NY, USA
*Corresponding authors: H.I.I. h.i.ingolfsson@rug.nl, J.T.S. jsack@ucdavis.edu, and O.S.A sparre@med.cornell.edu

Supporting Information Provided:

Additional Methods

Molecular dynamics force field details

Topologies compatible with the Martini[1,2] coarse-grain (CG) model were built for all five phytochemicals used in this work. CG to atomistic structural mapping, shown in Supporting Fig. S5, was chosen according to the chemical composition of the compounds. The chemical nature of the underlying atomistic building blocks guide the selection of appropriate CG bead types to best match the atomistic properties[2]. Bond, angle and dihedral potentials were calibrated to reproduce the corresponding distributions extracted from atomistic resolution simulations. The GROMOS 53A6[3] force field was used in the atomistic simulations and the topologies were generated for all the phytochemicals using the Automated force field Topology Builder (ATB)[4]. Each compound was simulated for 100 ns in a box of SPC water using the GROMACS 4.x simulation package[5,6] and standard GROMOS 53A6[3] parameters e.g. 2 fs time step, Berendsen thermostat (310 K, τ_T = 0.1 ps) and barostat (1 bar, κ_P = 4.6e^{-5} bar^{-1}, τ_P = 0.5 ps)[7], and the relative permittivity of the reaction-field set to 62. The CG Martini topologies can be found via www.cgmartini.nl.

Molecular dynamics simulation details

All CG simulations were done using the GROMACS 4.x simulation package[5,6], a time step of t = 20 fs and the standard Martini simulation parameters[1,2]. The temperature and pressure were controlled using the Berendsen thermostat and barostat[7]. The temperature was kept at 310 K with a τ_T = 1.0 ps and the pressure at 1 bar using a semi-isotropic pressure scheme with compressibility κ_P = 3e^{-4} bar^{-1} and relaxation time τ_P = 2.0 ps. For calculating the phytochemicals bilayer density and changes to the lateral pressure profile the phytochemicals were placed in the water phase above a pre-equilibrated CG 1-palmitoyl-2-oleoyl-*sn*-glycero-3-phosphocholine (POPC) bilayer in a 1:10 lipid to phytochemical mol ratio. Each simulation was run for 2.5 μs and the last 2 μs were used for analysis. Bilayer thickness was measured as the average distance between the POPC phosphate (PO4) head group beads in the opposing bilayer leaflets and the area per lipid as the average bilayer area divided by the number of lipids per leaflet. Average tail order is the average second-rank order parameter (P_2) for the tail and tail lipid backbone bonds. The P_2 and apparent area compressibility (K_A) were calculated as described by Marrink et al.[1], without correcting for membrane undulations. The lateral pressure profiles were determined using a modified version of the GROMACS package, which is available via www.gromacs.org and follows a formalism described previously[8,9]. Briefly, the lateral pressure, $\pi(z)$, may be obtained as the difference between the lateral, P_L, and normal, P_N, components of pressure tensor, that is: $P_L=(P_{XX}+P_{YY})/2$ and $P_N=P_{ZZ}$. In practice the system is first divided into a 3D grid with a 0.3 nm cell size. The local pressure tensor is then analyzed for each grid point and averages are calculated for x,y plane along the normal of the bilayer (z-axis). The bilayer bending modulus (K_c) was estimated using Evans polymer brush model[10], according to the formula $K_c=(K_A\text{*}(\text{bilayer thickness})^2)/24$, and the lipid spontaneous curvature (K_{0m}) and the bilayer elastic ratio are based on the first and second moments of the lateral pressure profile, as described in[11], see results in Supporting Table S2.

To quantify the phytochemicals' changes to the bilayer deformation energy the potential of mean force (PMF) of dragging a large bead across a CG POPC bilayer was measured, with and without the phytochemicals. A Lennard-Jones (LJ) particle was used as a probe and was designed to interact strongly with the Martini beads representing the choline, phosphate and glycerol groups in POPC (Q0, Qa and Na bead types) and weakly with everything else (including all the phytochemicals). The LJ parameters are $\sigma = 0.92$ nm for both the weak and strong interactions and $\varepsilon = 5.0$ and 200 kJ/mol for the weak and strong interactions, respectively. Note, however, that due to the shift function used with Martini[2,12], the effective deepest well depths are 0.12 and 4.62 kJ/mol for the weak and the strong interactions, at a bead-to-bead distance of r = 1.07 nm. The pulling simulations were run with the same parameters as described above, except that the velocity rescale thermostat[13] (T = 298 K, $\tau_t = 1.0$ ps) and Parrinello-Rahman barostat (P = 1.0 bar, $\tau_p = 4.0$ ps) was used. The initial bilayer patch was created using an in-house script (*insane.py*) and consisted of 132 lipids in both monolayers at a hydration level of ~50 waters

(~12.5 CG water beads) per lipid. 13 phytochemical molecules were added to each monolayer, ~10 mol%. Systems were equilibrated for 500 ns with the probe restrained at the starting position (4 nm from the bilayer center). Next, the probe was pulled through the bilayer at a rate of $8 \cdot 10^{-5}$ nm/ps, using a harmonic restraining potential of 1000 kJ/(mol nm^2). From these simulations 81 frames were extracted with the probe particle equally spaced between -4 – 4 nm distance from the bilayer center. These frames were subsequently used as starting structures for 100 ns simulations at each PMF window, during which the bead was restrained at a constant position using the same harmonic potential. The windows were analyzed using the implementation of the weighted histogram method (WHAM) as described in[14]. The Bayesian histogram bootstrapping method was applied, using 100 bootstrap iterations, where the histograms are weighted with their respective autocorrelation times. The profiles were set to zero and symmetrized around the bilayer center. The statistical errors obtained from the WHAM analyses can be considered as a lower bound for the error, however a better indication might be the asymmetry in unsymmetrized profiles (Supporting Fig. S2c). When pulling the probe through the bilayer a few phytochemicals occasionally flip between the leaflets (monolayers), see Supporting Fig. S2a. On average, for all windows, the ratio of phytochemicals in the leaflets is close to unity (Supporting Fig. S2a legend). To check for lateral rearrangement of the phytochemicals when the probe enters the bilayer we looked at the radial distribution function of the phytochemical in the XY-plane with respect to the probe. The averaged windows for when the probe was in the bilayer interface or in the aqueous phase, Supporting Fig. S2d shows this for resveratrol. For all the phytochemicals the XY-distribution is flat before the probe comes close to the bilayer. When the probe is at the bilayer interface the phytochemicals redistribute away from the probe. In these simulations we were not able to measure any significant accumulation of phytochemicals around the probe. Phytochemical preferential orientation relative to the probe was also not observed.

To check the distribution of the phytochemicals in the bilayer, and their effects on bilayer properties as estimated from the CG simulations, short POPC atomistic simulations were run without and with the phytochemical (at a 1:10 phytochemical to lipid molar ratio). The same atomistic parameter and force fields described in the *Molecular dynamics force field details section*, above, were used with the addition of POPC parameters, which were generously provided by Alex H. Vries (topologies available on demand). The last frame of the 2.5 ms long CG simulations was backmapped into atomistic coordinates using the reverse transformation method of Wassenaar et al.[15] and each condition simulated for 250 ns. Average properties were calculated from the last 200 ns of the simulation in the same manner as in the CG simulations except the phosphate-phosphate distance was used to estimate bilayer thickness. Lateral density profiles are shown in Supporting Fig. S3 and all average bilayer properties are reported in Supporting Table S2 (provided in a separate Excel file). Please note the phytochemicals force field were generated by ATB with little manual curation and therefore these simulations should only be considered as support for the CG results and to provide an overall indication of the bilayer effects of the phytochemicals and not as detailed studies on their nature.

Continuum model estimates

The required changes in bilayer material properties to increase gA function by 10 fold were estimated using the continuum elastic model of Nielsen and Andersen[16,17]. A changes in gA rate, $\Delta G_{\text{bilayer}}^{\text{M}\rightarrow\text{D}}$ (free energy difference for the transition between gA monomers and dimmers) of 10, meaning that $\Delta\Delta G_{\text{bilayer}}^{\text{M}\rightarrow\text{D}}$ is changed be <6 kJ mole^{-1}. In a bilayer with a bilayer hydrophobic thickness of 3.4 nm[18] (the $DC_{22:1}PC$ vesicles in the gA based fluorescence assay), a gA dimer with a hydrophobic length of the 2.2 nm[19-21], a bilayer spring constant (H_B) of ~100 kJ (mole·nm^2)$^{-1}$, a contact slope at inclusion-bilayer boundary (s) of 0, and the other parameters as described in[17] the $\Delta G_{\text{bilayer}}^{\text{M}\rightarrow\text{D}}$ is ~140 kJ mole^{-1}. From the continuum elastic model, if we look at changes in a few of the bilayer material properties in isolation: H_B needs to change by only ~4% to account for the observed results, the hydrophobic thickness by ~1%, the area compressibility (K_A) by ~5%, and the bilayer bending modulus (K_c) by ~10%. Which is in line with the modest changes in average bilayer properties observed in the MD simulations. By using the phytochemicals average change in bilayer properties from the CG simulations (a reduction in bilayer thickness by ~1%, K_A by ~4% and K_c by ~5%) the continuum elastic model predicts a reduction in $\Delta G_{\text{bilayer}}^{\text{M}\to\text{D}}$ by ~12 kJ mole^{-1}.

Additional Discussion

Membrane Protein-Lipid Bilayer Coupling

Changes in membrane protein reflect changes in the energetic (and kinetics) of protein conformational transitions. Limiting the discussion to the energetics, the free energy difference for the transition between two protein conformations, I and II, ($\Delta G_{\text{total}}^{\text{I}\mapsto\text{II}}$) is the sum of energetic contributions from rearrangements within the protein ($\Delta G_{\text{protein}}^{\text{I}\mapsto\text{II}}$) and from the ensuing different packing of the surrounding lipid bilayer, e.g.[22,23], ($\Delta G_{\text{bilayer}}^{\text{I}\mapsto\text{II}} = \Delta G_{\text{def}}^{\text{II}} - \Delta G_{\text{def}}^{\text{I}}$), where ΔG_{def} denotes the bilayer deformation energy associated with each membrane protein conformer. The phytochemicals alter $\Delta G_{\text{def}}^{\text{I}}$ (and $\Delta G_{\text{def}}^{\text{II}}$) when they partition into the lipid bilayer/solution interface[24-27]. The phytochemical-imposed changes in membrane protein function thus will depend not only on any changes in $\Delta G_{\text{protein}}^{\text{I}\mapsto\text{II}}$, but also on the changes in the protein/bilayer boundary associated with the conformational transitions underlying protein function, as well as the specific lipid environment—that is, the relative changes in $\Delta G_{\text{def}}^{\text{I}}$ and $\Delta G_{\text{def}}^{\text{II}}$, and thus the *change* in $\Delta G_{\text{bilayer}}^{\text{I}\mapsto\text{II}}$. It therefore is not surprising that the magnitude, and even the direction, of the changes in a given phytochemical's effects will vary among different membrane proteins.

Only in the case of the gramicidin, and maybe the MscL, channels is there sufficient information about the transitions underlying the changes in channel function to allow a more detailed interpretation. In the case of the gramicidin channels, the hydrophobic length of the conducting channels (~2.2 nm[19-21]) is less than the host bilayer hydrophobic thickness (4.0 nm for $DC_{18:1}PC$/*n*-decane planar bilayers[27] and 3.4 nm for the hydrocarbon-free $DC_{22:1}PC$ membranes [18]), and increases in bilayer elasticity will decrease the bilayer contribution to the free energy of dimerization. In the case of MscL, the hydrophobic length of the open state of the channel is less than that of the closed state, (cf. [28-30]. One would thus expect that the phytochemical-induced increases in lipid bilayer elasticity would stabilize the open state, contrary to what is observed. The most likely reason for this "discrepancy" is that the phytochemicals increase in the energetic cost of increasing the MscL cross-sectional area that is associated with channel opening[31].

Table S1. Membrane proteins known to be affected by phytochemicals[a]

	Capsaicin	Curcumin	EGCG	Genistein	Resveratrol
5-Hydroxytryptamine receptor 3A (5-HT3A)					+[32]
ATP-sensitive K^+ channels (K_{ATP})		*[33]	-[34]	±[35,36]	-[37]
Ca^{2+} release-activated Ca^{2+} channel (CRAC)	-[38]	-[39]			
Cystic fibrosis transmembrane conductance regulator (CFTR)	+[40]	+[41-44]		±[45,46]	+[47]
Epidermal growth factor receptor (EGFR / HER)	±[48,49]	-[50,51]	*/-[52,53]	-[54]	*[55]
Estrogen Receptor		*[56]	*[57]	*[58]	*[59,60]
Fibroblast growth factor receptor (FGFR)			-[53]	*[61]	
F_OF_1-ATPase/ATP synthase		-[62]	-[62]	-[62]	-[62]
Glycine receptors				-[63]	
Gramicidin A (gA)	+[64,CA]	+[65,CA]	+[52,66, CA]	+[67,CA]	+[CA]
hERG K^+ channels	-[68]	-[69,70]	-[71]	-[72]	
Human epidermal growth factor receptor 2 (ErbB2/HER2)	*[73]	-[74]	-[53]	-[75]	-[76]
Ileal apical Na^+ bile acid transporter (ASBT)			-[77]		
Inositol triphosphate receptor (InsP3R)		-[78]			
Insulin receptors (IR)		+[79]			
Insulin-like growth factor-1 receptor (IGF-1R)			-[53]		
Kir2.3 inwardly-rectifying K^+ channel				-[80]	
$K_V1.1$ K^+ channels	-[81]				*[82]
$K_V1.2$ K^+ channels	-[81]				
$K_V1.3$ K^+ channels	-[81]	-[83]		-[84]	-[85]
$K_V1.4$ K^+ channels		-[86]		-[87]	
$K_V1.5$ K^+ channels	-[81]		-[88]	-[88]	*[89]
$K_V2.1$ K^+ channels	-[CA]	-[CA]	-[CA]	-[CA]	
$K_V3.1$ K^+ channels	-[81]				
$K_V4.3$ K^+ channels				-[90]	
$K_V7.1$ K^+ channels - KvLQT1/minK			-[91]		
L-type Ca^{2+} channels	±[92]	-[93]	-[91]	-[94]	-[95]
Large-conductance Ca^{2+} activated K^+ channels (BK/Maxi-K)	*[96]			+[97]	+[98]

Mechanosensitive channels of large conductance (MscL)	–[CA]	–[CA]	–[CA]	–[CA]	–[CA]
Membrane-anchored disintegrin-type metalloproteinase (ADAM17)	–[CA]				
Mitochondrial permeability transition pore (MPTP)		+[99,100]		+[101]	+[102]
Na^+/Ca^{2+} exchanger			±[103,104]		
Na^+/H^+ exchanger			+[103]		
P-glycoprotein (Pgp) / ABC-transporter	±[105,106]	–[105,107-109]	–[110]	–[106]	–[105]
Peroxisome proliferator-activated receptor-γ (PPARγ)		+[51]			
Platelet-derived growth factor receptor (PDGF-R)		–[111]	–[53]	–[112]	–[113]
Ryanodine receptor type 2 (RyR2)			+[104]		
Sarco/endoplasmic reticulum Ca^{2+} ATPase (SERCA)	*[114]	–[115]	±[116]		*[117]
Small conductance K^+ channel (SK)				+[118]	
Transient receptor potential (TRP) channels	+[119,120,121,122]	+[123,124]	+[125]	+[126]	–[127]
Two-pore K^+ channels (KCNK)		–[128,129]		–[130]	
Vascular endothelial growth factor (VEGF)		–[131]	–[53,132,133]	–[134]	–[133]
Voltage-sensitive Na^+ channels (Na_V)	–[64,135-137, CA]		–[91,138, CA]	–[139,CA]	–[140,CA]
β_2-adrenoceptor		+[79]			

[a]Phytochemicals alter the function of many different membrane proteins. This table provides only an overview of the range of effects because the selected five phytochemicals are extensively studied (with hundreds of publications per year for each compound) and some reported membrane protein interactions are therefore missing. (+) indicates activation or up-regulation, (–) indicates inhibition or down-regulation, (*) indicates "interaction," (±) indicates biphasic dose response curve or both activation and inhibition reported and no symbol means that we are not aware of existing data. The phytochemicals' reported activity is followed by original articles and/or review article citation or CA for current article.

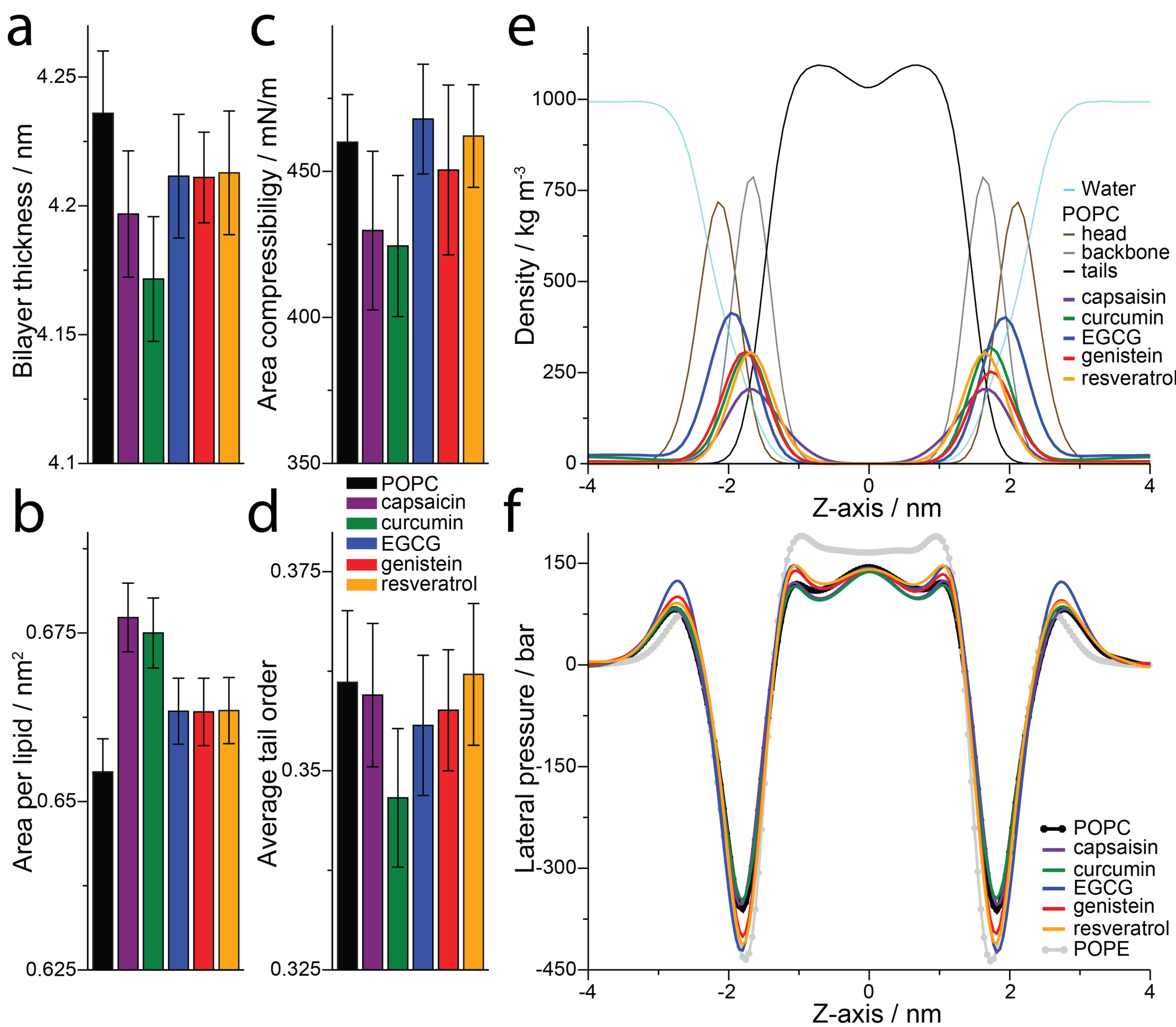

Figure S1. Phytochemicals alter the physical properties of simulated phospholipid bilayers. The phytochemicals' effects on CG 1-palmitoyl-2-oleoyl-sn-glycero-3-phosphocholine (POPC) bilayers were explored using CG Martini simulations at 1:10 lipid mol ratio. (a-d) Bulk bilayer properties, avg ± sd. (e) Lateral density of equilibrium simulations. For clarity, the density of POPC head and backbone are scaled by 1.5 and the phytochemicals are scaled by 2. (f) POPC lateral pressure profiles with and without phytochemicals, also showing the pressure profile for CG 1-palmitoyl-2-oleoyl-sn-glycero-3-phosphoethanolamine (POPE) for comparison.

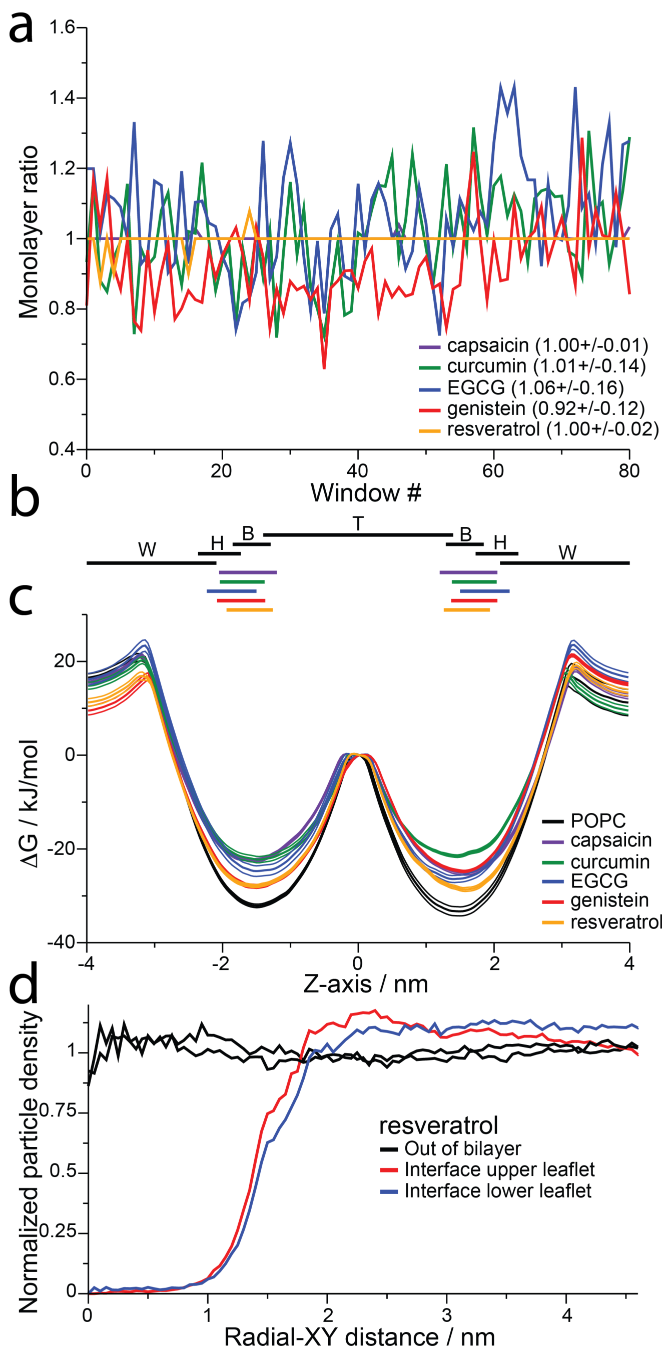

Figure S2. Phytochemicals reduced the energy required to perturb bilayers. To evaluate the phytochemicals' effect on the energy required to perturb the bilayer a large bead (radius 0.9 nm) was dragged across a CG POPC bilayer with and without 1:10 lipid mol ratio of the phytochemicals and the PMF calculated. (a) Ratio of phytochemicals between the two monolayers (leaflets) for each window of the potential of mean force (PMF) simulations. Avg ±

sd across all windows are listed for each phytochemical. (b) Lateral density, indicated as density width at half maximum, shown for: water (W), POPC lipid head groups (H), backbone (B), tails (T) and for the phytochemicals. Calculated across all windows of the PMF simulations. (c) Unsymmetrized PMF for dragging the bead through the bilayer. The bilayer normal is set to the Z-axis with zero at the center of the bilayer. (d) Radial distribution function of the resveratrol molecules in the XY-plane with respect to the probe (the large bead). Out of the bilayer (black) curves are averages over PMF windows 0-8 and 72-80 where the probe is far enough out of the bilayer to not influence the distribution of the phytochemicals. The upper (red) and lower (blue) leaflet interface curves represent resveratrol molecules in the upper and lower leaflet when the probe is in the corresponding leaflet.

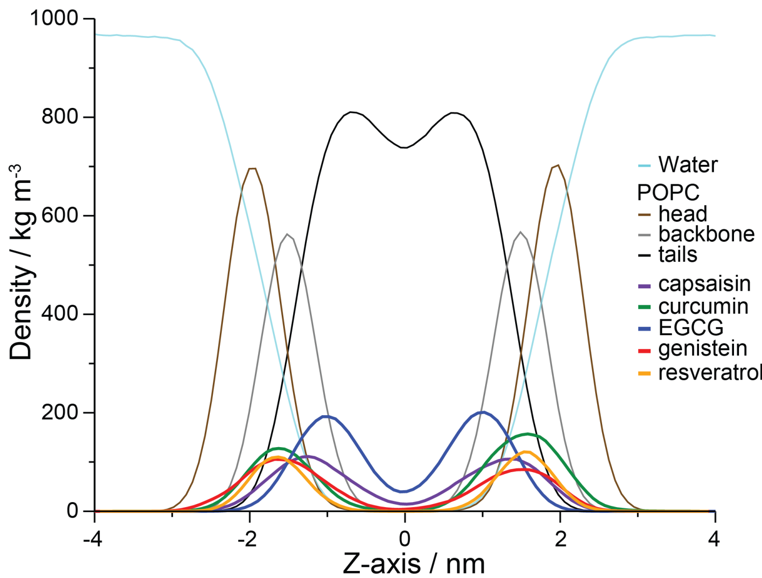

Figure S3. Bilayer localization of the phytochemicals from atomistic simulations. Lateral density of the phytochemicals embedded in a POPC bilayer 1:10 lipid mol ratio, results from atomistic simulations. For clarity, the density of POPC head and backbone are scaled by 1.5 and the phytochemicals are scaled by 2.

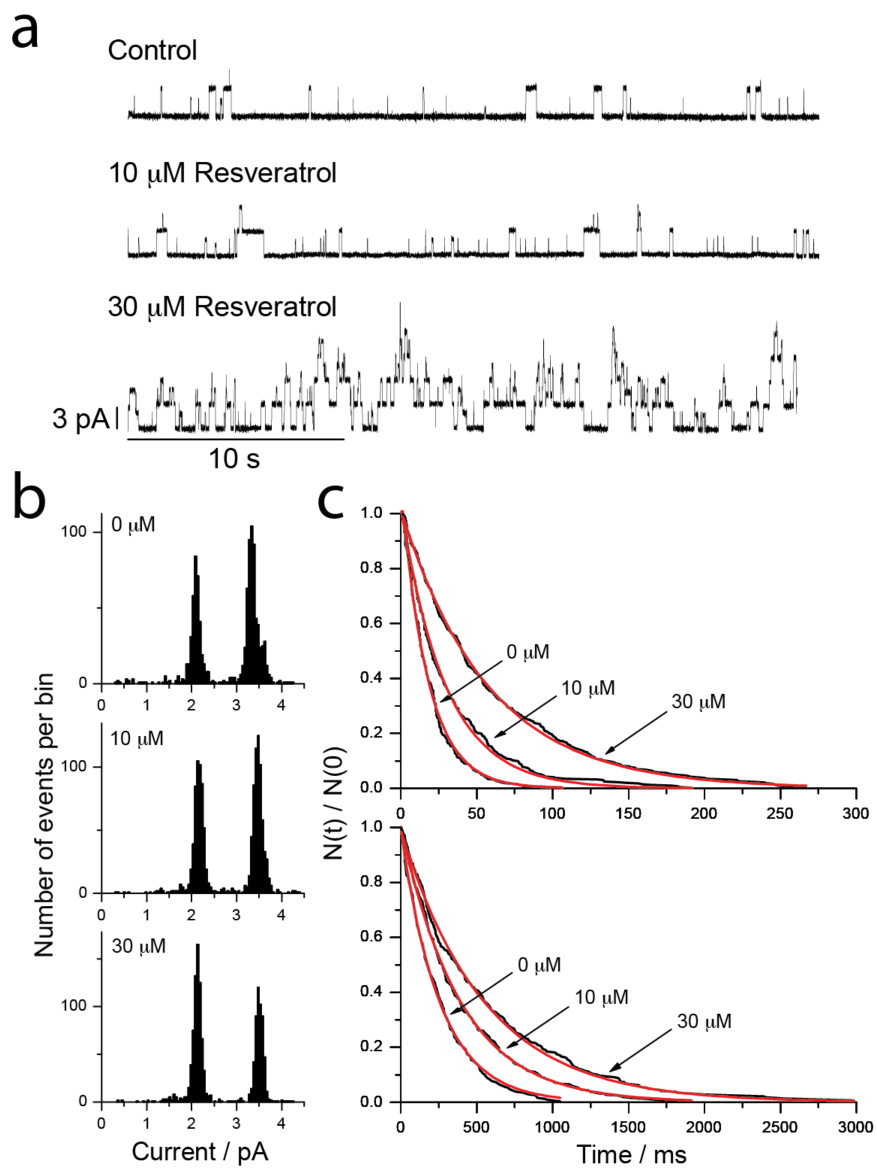

Figure S4. Effects of resveratrol on gA channel activity. (a) Single channel current traces showing gA channel activity in DOPC/*n*-decane bilayer with 0, 10 and 30 μM resveratrol. (b) Current transition amplitude histogram with 0, 10 and 30 μM resveratrol for $gA^{-}(13)$ (left peak) and AgA(15) (right peak). (c) Normalized single channel survivor histograms for $gA^{-}(13)$ (top) and AgA(15) (bottom), fitted with a single exponential distribution (red line) given by $N(t)/N(0) = \exp\{-t/\tau\}$. 1.0 M NaCl, 10 mM HEPES pH 7.0, 25 °C, ±200 mV, 500 Hz.

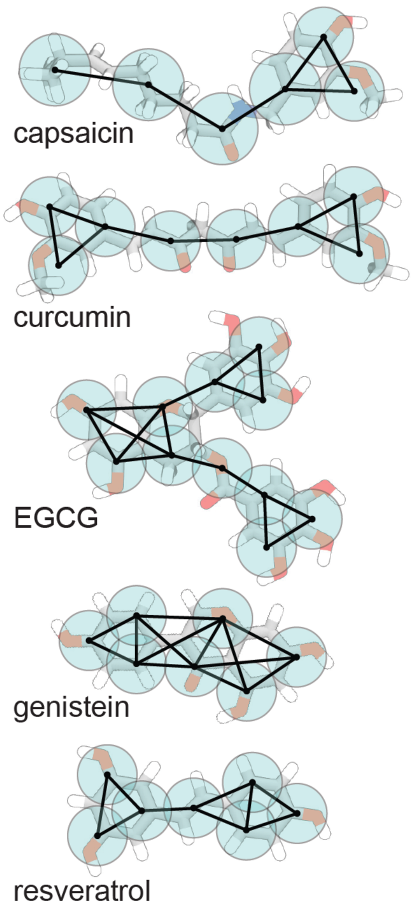

Figure S5. CG mapping schema for the phytochemicals. For each of the five phytochemicals the CG Martini representation is shown on top of the atomistic structure. The CG beads (cyan spheres) are placed roughly at the center of the group of atoms they represent. All CG bonds are depicted with a black line.

Additional References

(1) Marrink, S. J., De Vries, A. H., and Mark, A. E. (2004) Coarse grained model for semiquantitative lipid simulations. *J. Phys. Chem. B 108*, 750–760.
(2) Marrink, S. J., Risselada, H. J., Yefimov, S., Tieleman, D. P., and De Vries, A. H. (2007) The MARTINI force field: coarse grained model for biomolecular simulations. *J. Phys. Chem. B 111*, 7812–7824.
(3) Oostenbrink, C., Villa, A., Mark, A. E., and van Gunsteren, W. F. (2004) A biomolecular force field based on the free enthalpy of hydration and solvation: the GROMOS force-field parameter sets 53A5 and 53A6. *J. Comput. Chem. 25*, 1656–1676.
(4) Malde, A. K., Zuo, L., Breeze, M., Stroet, M., Poger, D., Nair, C. P., Oostenbrink, C., Mark, A. E., and E, A. (2011) An automated force field topology builder (ATB) and repository: version 1.0. *J. Chem. Theory Comput. 7*, 4026–4037.
(5) Hess, B., Kutzner, C., van der Spoel, D., and Lindahl, E. (2008) GROMACS 4: algorithms for highly efficient, load-balanced, and scalable molecular simulation. *J. Chem. Theory Comput. 4*, 435–447.
(6) Pronk, S., Pall, S., Schulz, R., Larsson, P., Bjelkmar, P., Apostolov, R., Shirts, M. R., Smith, J. C., Kasson, P. M., van der Spoel, D., Hess, B., and Lindahl, E. (2013) GROMACS 4.5: a high-throughput and highly parallel open source molecular simulation toolkit. *Bioinformatics 29*, 845–854.
(7) Berendsen, H., and Postma, J. (1984) Molecular dynamics with coupling to an external bath. *J. Chem. Phys. 81*, 3684–3690.
(8) Lindahl, E., and Edholm, O. (2000) Spatial and energetic-entropic decomposition of surface tension in lipid bilayers from molecular dynamics simulations. *J. Chem. Phys. 113*, 3882–3893.
(9) Ollila, O. H., Risselada, H. J., Louhivuori, M., Lindahl, E., Vattulainen, I., and Marrink, S. J. (2009) 3D pressure field in lipid membranes and membrane-protein complexes. *Phys. Rev. Lett. 102*, 078101.
(10) Rawicz, W., Olbrich, K. C., McIntosh, T., Needham, D., and Evans, E. (2000) Effect of chain length and unsaturation on elasticity of lipid bilayers. *Biophys. J. 79*, 328–339.
(11) Hu, M., de Jong, D. H., Marrink, S. J., and Deserno, M. (2013) Gaussian curvature elasticity determined from global shape transformations and local stress distributions: a comparative study using the MARTINI model. *Faraday Discuss. 161*, 365–82– discussion 419–59.
(12) Baron, R., Trzesniak, D., De Vries, A. H., Elsener, A., Marrink, S. J., and van Gunsteren, W. F. (2007) Comparison of Thermodynamic Properties of Coarse-Grained and Atomic-Level Simulation Models. *Chem. Phys. Chem. 8*, 452–461.
(13) Bussi, G., Donadio, D., and Parrinello, M. (2007) Canonical sampling through velocity rescaling. *J. Chem. Phys. 126*, 014101.
(14) Hub, J. S., de Groot, B. L., and van der Spoel, D. (2013) g_wham— A Free Weighted Histogram Analysis Implementation Including Robust Error and Autocorrelation Estimates. *J. Chem. Theory Comput. 6*, 3713–3720.
(15) Wassenaar, T. A., Pluhackova, K., Böckmann, R. A., Marrink, S. J., and Tieleman, D. P. (2014) Going Backward: A Flexible Geometric Approach to Reverse Transformation from Coarse Grained to Atomistic Models. *J. Chem. Theory Comput. 10*, 676–690.
(16) Nielsen, C., Goulian, M., and Andersen, O. S. (1998) Energetics of inclusion-induced bilayer deformations. *Biophys. J. 74*, 1966–1983.
(17) Nielsen, C., and Andersen, O. S. (2000) Inclusion-induced bilayer deformations: effects of

monolayer equilibrium curvature. *Biophys. J. 79*, 2583–2604.
(18) Lewis, B. A., and Engelman, D. M. (1983) Lipid bilayer thickness varies linearly with acyl chain length in fluid phosphatidylcholine vesicles. *J. Mol. Biol. 166*, 211–217.
(19) Elliott, J. R., Needham, D., Dilger, J. P., and Haydon, D. A. (1983) The effects of bilayer thickness and tension on gramicidin single-channel lifetime. *Biochim. Biophys. Acta 735*, 95–103.
(20) Huang, H. W. (1986) Deformation free energy of bilayer membrane and its effect on gramicidin channel lifetime. *Biophys. J. 50*, 1061–1070.
(21) Harroun, T. A., Heller, W. T., Weiss, T. M., Yang, L., and Huang, H. W. (1999) Experimental evidence for hydrophobic matching and membrane-mediated interactions in lipid bilayers containing gramicidin. *Biophys. J. 76*, 937–945.
(22) Andersen, O. S., Nielsen, C., Maer, A. M., Lundbæk, J. A., Goulian, M., and Koeppe, R. E., II. (1999) Ion channels as tools to monitor lipid bilayer-membrane protein interactions: gramicidin channels as molecular force transducers. *Meth. Enzymol. 294*, 208–224.
(23) Lundbæk, J. A., Collingwood, S. A., Ingólfsson, H. I., Kapoor, R., and Andersen, O. S. (2010) Lipid bilayer regulation of membrane protein function: gramicidin channels as molecular force probes. *J. R. Soc. Interface 7*, 373–395.
(24) Szleifer, I., Ben-Shaul, A., and Gelbart, W. M. (1990) Chain packing statistics and thermodynamics of amphiphile monolayers. *J. Phys. Chem. 94*, 5081–5089.
(25) Evans, E., Rawick, W., and Hofmann, A. F. (1995) Lipid bilayer expansion and mechanical disruption in solutions of water-soluble bile acid. *Falk Symposium* 59–68.
(26) Zhelev, D. V. (1998) Material property characteristics for lipid bilayers containing lysolipid. *Biophys. J. 75*, 321–330.
(27) Lundbæk, J. A., Koeppe, R. E., II, and Andersen, O. S. (2010) Amphiphile regulation of ion channel function by changes in the bilayer spring constant. *Proc. Natl. Acad. Sci. U.S.A. 107*, 15427–15430.
(28) Chang, G., Spencer, R. H., Lee, A. T., Barclay, M. T., and Rees, D. C. (1998) Structure of the MscL homolog from Mycobacterium tuberculosis: a gated mechanosensitive ion channel. *Science 282*, 2220–2226.
(29) Sukharev, S., Betanzos, M., Chiang, C. S., and Guy, H. R. (2001) The gating mechanism of the large mechanosensitive channel MscL. *Nature 409*, 720–724.
(30) Perozo, E., Kloda, A., Cortes, D. M., and Martinac, B. (2002) Physical principles underlying the transduction of bilayer deformation forces during mechanosensitive channel gating. *Nat. Struct. Biol. 9*, 696–703.
(31) Ollila, O. H. S., Louhivuori, M., Marrink, S. J., and Vattulainen, I. (2011) Protein shape change has a major effect on the gating energy of a mechanosensitive channel. *Biophys. J. 100*, 1651–1659.
(32) Lee, B.-H., Hwang, S.-H., Choi, S.-H., Shin, T.-J., Kang, J., Lee, S.-M., and Nah, S.-Y. (2011) Resveratrol enhances 5-hydroxytryptamine type 3A receptor-mediated ion currents: the role of arginine 222 residue in pre-transmembrane domain I. *Biol. Pharm. Bull. 34*, 523–527.
(33) De Paz-Campos, M. A., Chávez-Piña, A. E., Ortiz, M. I., and Castañeda-Hernández, G. (2012) Evidence for the Participation of ATP-sensitive Potassium Channels in the Antinociceptive Effect of Curcumin. *Korean J. Pain 25*, 221–227.
(34) Jin, J.-Y., Park, S.-H., Bae, J.-H., Cho, H.-C., Lim, J.-G., Park, W. S., Han, J., Lee, J. H., and Song, D.-K. (2007) Uncoupling by (−)-epigallocatechin-3-gallate of ATP-sensitive potassium channels from phosphatidylinositol polyphosphates and ATP. *Pharmacol. Res. 56*,

237–247.
(35) Kwak, Y. G., Park, S. K., Cho, K. P., and Chae, S. W. (1996) Reciprocal modulation of ATP-sensitive K+ channel activity in rat ventricular myocytes by phosphorylation of tyrosine and serine/threonine residues. *Life Sci. 58*, 897–904.
(36) Ogata, R., Kitamura, K., Ito, Y., and Nakano, H. (1997) Inhibitory effects of genistein on ATP-sensitive K+ channels in rabbit portal vein smooth muscle. *Br. J. Pharmacol. 122*, 1395–1404.
(37) Chen, W.-P., Chi, T.-C., Chuang, L.-M., and Su, M.-J. (2007) Resveratrol enhances insulin secretion by blocking K(ATP) and K(V) channels of beta cells. *Eur. J. Pharmacol. 568*, 269–277.
(38) Fischer, B. S., Qin, D., Kim, K., and McDonald, T. V. (2001) Capsaicin inhibits Jurkat T-cell activation by blocking calcium entry current I(CRAC). *J. Pharmacol. Exp. Ther. 299*, 238–246.
(39) Shin, D. H., Seo, E. Y., Pang, B., Nam, J. H., Kim, H. S., Kim, W. K., and Kim, S. J. (2011) Inhibition of Ca2+-release-activated Ca2+ channel (CRAC) and K+ channels by curcumin in Jurkat-T cells. *J. Pharmacol. Sci. 115*, 144–154.
(40) Ai, T., Bompadre, S. G., Wang, X., Hu, S., Li, M., and Hwang, T. C. (2004) Capsaicin potentiates wild-type and mutant cystic fibrosis transmembrane conductance regulator chloride-channel currents. *Mol. Pharmacol. 65*, 1415–1426.
(41) Egan, M. E., Pearson, M., Weiner, S. A., Rajendran, V., Rubin, D., Glockner-Pagel, J., Canny, S., Du, K., Lukacs, G. L., and Caplan, M. J. (2004) Curcumin, a major constituent of turmeric, corrects cystic fibrosis defects. *Science 304*, 600–602.
(42) Berger, A. L., Randak, C. O., Ostedgaard, L. S., Karp, P. H., Vermeer, D. W., and Welsh, M. J. (2005) Curcumin stimulates cystic fibrosis transmembrane conductance regulator Cl-channel activity. *J. Biol. Chem. 280*, 5221–5226.
(43) Wang, W., Li, G., Clancy, J. P., and Kirk, K. L. (2005) Activating cystic fibrosis transmembrane conductance regulator channels with pore blocker analogs. *J. Biol. Chem. 280*, 23622–23630.
(44) Wang, W., Bernard, K., Li, G., and Kirk, K. L. (2007) Curcumin opens cystic fibrosis transmembrane conductance regulator channels by a novel mechanism that requires neither ATP binding nor dimerization of the nucleotide-binding domains. *J. Biol. Chem. 282*, 4533–4544.
(45) Illek, B., Fischer, H., and Machen, T. E. (1996) Alternate stimulation of apical CFTR by genistein in epithelia. *Am. J. Physiol. 270*, C265–275.
(46) Wang, F., Zeltwanger, S., Yang, I. C. H., Nairn, A. C., and Hwang, T. C. (1998) Actions of genistein on cystic fibrosis transmembrane conductance regulator channel gating. evidence for two binding sites with opposite effects. *J. Gen. Physiol. 111*, 477–490.
(47) Alexander, N. S., Hatch, N., Zhang, S., Skinner, D., Fortenberry, J., Sorscher, E. J., and Woodworth, B. A. (2011) Resveratrol has salutary effects on mucociliary transport and inflammation in sinonasal epithelium. *Laryngoscope 121*, 1313–1319.
(48) Hwang, M. K., Bode, A. M., Byun, S., Song, N. R., Lee, H. J., Lee, K. W., and Dong, Z. (2010) Cocarcinogenic effect of capsaicin involves activation of EGFR signaling but not TRPV1. *Cancer Res. 70*, 6859–6869.
(49) Hwang, Y. P., Yun, H. J., Choi, J. H., Han, E. H., Kim, H. G., Song, G. Y., Kwon, K.-I., Jeong, T. C., and Jeong, H. G. (2011) Suppression of EGF-induced tumor cell migration and matrix metalloproteinase-9 expression by capsaicin via the inhibition of EGFR-mediated FAK/Akt, PKC/Raf/ERK, p38 MAPK, and AP-1 signaling. *Mol. Nutr. Food Res. 55*, 594–605.

(50) Chen, A., and Xu, J. (2005) Activation of PPAR{gamma} by curcumin inhibits Moser cell growth and mediates suppression of gene expression of cyclin D1 and EGFR. *Am. J. Physiol. Gastrointest. Liver Physiol. 288*, G447–456.
(51) Chen, A., Xu, J., and Johnson, A. C. (2006) Curcumin inhibits human colon cancer cell growth by suppressing gene expression of epidermal growth factor receptor through reducing the activity of the transcription factor Egr-1. *Oncogene 25*, 278–287.
(52) Adachi, S., Nagao, T., Ingólfsson, H. I., Maxfield, F. R., Andersen, O. S., Kopelovich, L., and Weinstein, I. B. (2007) The inhibitory effect of (-)-epigallocatechin gallate on activation of the epidermal growth factor receptor is associated with altered lipid order in HT29 colon cancer cells. *Cancer Res. 67*, 6493–6501.
(53) Shimizu, M., Shirakami, Y., and Moriwaki, H. (2008) Targeting Receptor Tyrosine Kinases for Chemoprevention by Green Tea Catechin, EGCG. *Int. J. Mol. Sci. 9*, 1034–1049.
(54) Nakamura, H., Wang, Y., Kurita, T., Adomat, H., Cunha, G. R., and Wang, Y. (2011) Genistein increases epidermal growth factor receptor signaling and promotes tumor progression in advanced human prostate cancer. *PLoS ONE 6*, e20034.
(55) Herbert, K. J., and Snow, E. T. (2012) Modulation of arsenic-induced epidermal growth factor receptor pathway signalling by resveratrol. *Chem. Biol. Interact. 198*, 38–48.
(56) Bachmeier, B. E., Mirisola, V., Romeo, F., Generoso, L., Esposito, A., Dell'eva, R., Blengio, F., Killian, P. H., Albini, A., and Pfeffer, U. (2010) Reference profile correlation reveals estrogen-like trancriptional activity of Curcumin. *Cell. Physiol. Biochem. 26*, 471–482.
(57) Farabegoli, F., Barbi, C., Lambertini, E., and Piva, R. (2007) (−)-Epigallocatechin-3-gallate downregulates estrogen receptor alpha function in MCF-7 breast carcinoma cells. *Cancer Detect. Prev. 31*, 499–504.
(58) Bielecki, A., Roberts, J., Mehta, R., and Raju, J. (2010) Estrogen Receptor-beta Mediates the Inhibition of DLD-1 Human Colon Adenocarcinoma Cells by Soy Isoflavones. *Nutr. Cancer 63*, 139–150.
(59) Harikumar, K. B., and Aggarwal, B. B. (2008) Resveratrol: a multitargeted agent for age-associated chronic diseases. *Cell Cycle 7*, 1020–1035.
(60) Robb, E. L., and Stuart, J. A. (2011) Resveratrol interacts with estrogen receptor-beta to inhibit cell replicative growth and enhance stress resistance by upregulating mitochondrial superoxide dismutase. *Free Radic. Biol. Med.*
(61) Koroma, B. M., and de Juan, E. (1994) Phosphotyrosine inhibition and control of vascular endothelial cell proliferation by genistein. *Biochem. Pharmacol. 48*, 809–818.
(62) Zheng, J., and Ramirez, V. D. (2000) Inhibition of mitochondrial proton F0F1-ATPase/ATP synthase by polyphenolic phytochemicals. *Br. J. Pharmacol. 130*, 1115–1123.
(63) Huang, R. Q., and Dillon, G. H. (2000) Direct inhibition of glycine receptors by genistein, a tyrosine kinase inhibitor. *Neuropharmacology 39*, 2195–2204.
(64) Lundbæk, J. A., Birn, P., Tape, S. E., Toombes, G. E., Søgaard, R., Koeppe, R. E., II, Gruner, S. M., Hansen, A. J., and Andersen, O. S. (2005) Capsaicin regulates voltage-dependent sodium channels by altering lipid bilayer elasticity. *Mol. Pharmacol. 68*, 680–689.
(65) Ingólfsson, H. I., Koeppe, R. E., II, and Andersen, O. S. (2007) Curcumin is a modulator of bilayer material properties. *Biochemistry 46*, 10384–10391.
(66) Ingólfsson, H. I., Koeppe, R. E., II, and Andersen, O. S. (2011) Effects of green tea catechins on gramicidin channel function and inferred changes in bilayer properties. *FEBS Lett. 585*, 3101–3105.
(67) Hwang, T. C., Koeppe, R. E., II, and Andersen, O. S. (2003) Genistein can modulate

channel function by a phosphorylation-independent mechanism: importance of hydrophobic mismatch and bilayer mechanics. *Biochemistry 42*, 13646–13658.
(68) Xing, J., Ma, J., Zhang, P., and Fan, X. (2010) Block effect of capsaicin on hERG potassium currents is enhanced by S6 mutation at Y652. *Eur. J. Pharmacol. 630*, 1–9.
(69) Hu, C. W., Sheng, Y., Zhang, Q., Liu, H.-B., Xie, X., Ma, W.-C., Huo, R., and Dong, D.-L. (2012) Curcumin inhibits hERG potassium channels *in vitro*. *Toxicol. Lett. 208*, 192–196.
(70) Banderali, U., Belke, D., Singh, A., Jayanthan, A., Giles, W. R., and Narendran, A. (2011) Curcumin blocks Kv11.1 (erg) potassium current and slows proliferation in the infant acute monocytic leukemia cell line THP-1. *Cell. Physiol. Biochem. 28*, 1169–1180.
(71) Kelemen, K., Kiesecker, C., Zitron, E., Bauer, A., Scholz, E., Bloehs, R., Thomas, D., Greten, J., Remppis, A., Schoels, W., Katus, H. A., and Karle, C. A. (2007) Green tea flavonoid epigallocatechin-3-gallate (EGCG) inhibits cardiac hERG potassium channels. *Biochem. Biophys. Res. Commun. 364*, 429–435.
(72) Zhang, D.-Y., Wang, Y., Lau, C.-P., Tse, H.-F., and Li, G.-R. (2008) Both EGFR kinase and Src-related tyrosine kinases regulate human ether-à-go-go-related gene potassium channels. *Cell. Signal. 20*, 1815–1821.
(73) Thoennissen, N. H., O'Kelly, J., Lu, D., Iwanski, G. B., La, D. T., Abbassi, S., Leiter, A., Karlan, B., Mehta, R., and Koeffler, H. P. (2010) Capsaicin causes cell-cycle arrest and apoptosis in ER-positive and -negative breast cancer cells by modulating the EGFR/HER-2 pathway. *Oncogene 29*, 285–296.
(74) Tikhomirov, O., and Carpenter, G. (2001) Caspase-dependent cleavage of ErbB-2 by geldanamycin and staurosporin. *J. Biol. Chem. 276*, 33675–33680.
(75) Sakla, M. S., Shenouda, N. S., Ansell, P. J., Macdonald, R. S., and Lubahn, D. B. (2007) Genistein affects HER2 protein concentration, activation, and promoter regulation in BT-474 human breast cancer cells. *Endocrine 32*, 69–78.
(76) Choi, H. K., Yang, J. W., and Kang, K. W. (2006) Bifunctional effect of resveratrol on the expression of ErbB2 in human breast cancer cell. *Cancer Lett 242*, 198–206.
(77) Annaba, F., Kumar, P., Dudeja, A. K., Saksena, S., Gill, R. K., and Alrefai, W. A. (2010) Green tea catechin EGCG inhibits ileal apical sodium bile acid transporter ASBT. *Am. J. Physiol. Gastrointest. Liver Physiol. 298*, G467–G473.
(78) Dyer, J. L., Khan, S. Z., Bilmen, J. G., Hawtin, S. R., Wheatley, M., Javed, M. U., and Michelangeli, F. (2002) Curcumin: a new cell-permeant inhibitor of the inositol 1,4,5-trisphosphate receptor. *Cell Calcium 31*, 45–52.
(79) Xavier, S., Sadanandan, J., George, N., and Paulose, C. S. (2012) β2-Adrenoceptor and insulin receptor expression in the skeletal muscle of streptozotocin induced diabetic rats: Antagonism by vitamin D3 and curcumin. *Eur. J. Pharmacol. 687*, 14–20.
(80) Zhao, Z., Liu, B., Zhang, G., Jia, Z., Jia, Q., Geng, X., and Zhang, H. (2008) Molecular basis for genistein-induced inhibition of Kir2.3 currents. *Pflugers Arch - Eur. J. Physiol. 456*, 413–423.
(81) Grissmer, S., Nguyen, A. N., Aiyar, J., Hanson, D. C., Mather, R. J., Gutman, G. A., Karmilowicz, M. J., Auperin, D. D., and Chandy, K. G. (1994) Pharmacological characterization of five cloned voltage-gated K+ channels, types Kv1.1, 1.2, 1.3, 1.5, and 3.1, stably expressed in mammalian cell lines. *Mol. Pharmacol. 45*, 1227–1234.
(82) Novakovic, A., Gojkovic-Bukarica, L., Peric, M., Nezic, D., Djukanovic, B., Markovic-Lipkovski, J., and Heinle, H. (2006) The mechanism of endothelium-independent relaxation induced by the wine polyphenol resveratrol in human internal mammary artery. *J. Pharmacol.*

Sci. 101, 85–90.
(83) Lian, Y.-T., Yang, X.-F., Wang, Z.-H., Yang, Y., Yang, Y., Shu, Y.-W., Cheng, L.-X., and Liu, K. (2012) Curcumin Serves as a Human Kv1.3 Blocker to Inhibit Effector Memory T Lymphocyte Activities. *Phytother. Res.*
(84) Teisseyre, A., and Michalak, K. (2005) Genistein inhibits the activity of kv1.3 potassium channels in human T lymphocytes. *J. Membr. Biol. 205*, 71–79.
(85) Teisseyre, A., and Michalak, K. (2006) Inhibition of the activity of human lymphocyte Kv1.3 potassium channels by resveratrol. *J. Membr. Biol. 214*, 123–129.
(86) Liu, H., Danthi, S. J., and Enyeart, J. J. (2006) Curcumin potently blocks Kv1.4 potassium channels. *Biochem. Biophys. Res. Commun. 344*, 1161–1165.
(87) Zhang, Z.-H., and Wang, Q. (2000) Modulation of a cloned human A-type voltage-gated potassium channel (hKv1.4) by the protein tyrosine kinase inhibitor genistein. *Pflugers Arch - Eur. J. Physiol. 440*, 784–792.
(88) Choi, B. H. (2006) Effect of Genistein, a Tyrosine Kinase Inhibitor, on the Cloned Rat Brain Potassium Channel Kv1.5. *Korean J. Physiol. Pharmacol. 10*, 243–249.
(89) Ting, Y. K., Morikawa, K., Kurata, Y., Li, P., Bahrudin, U., Mizuta, E., Kato, M., Miake, J., Yamamoto, Y., Yoshida, A., Murata, M., Inoue, T., Nakai, A., Shiota, G., Higaki, K., Nanba, E., Ninomiya, H., Shirayoshi, Y., and Hisatome, I. (2011) Transcriptional activation of the anchoring protein SAP97 by heat shock factor (HSF)-1 stabilizes K(v) 1.5 channels in HL-1 cells. *Br. J. Pharmacol. 162*, 1832–1842.
(90) Kim, H. J., Ahn, H. S., Choi, B. H., and Hahn, S. J. (2011) Inhibition of Kv4.3 by genistein via a tyrosine phosphorylation-independent mechanism. *Am. J. Physiol. Cell Physiol. 300*, C567–C575.
(91) Kang, J., Cheng, H., Ji, J., Incardona, J., and Rampe, D. (2010) In Vitro Electrocardiographic and Cardiac Ion Channel Effects of (-)-Epigallocatechin-3-Gallate, the Main Catechin of Green Tea. *J. Pharmacol. Exp. Ther. 334*, 619–626.
(92) Hagenacker, T., Splettstoesser, F., Greffrath, W., Treede, R.-D., and Büsselberg, D. (2005) Capsaicin differentially modulates voltage-activated calcium channel currents in dorsal root ganglion neurones of rats. *Brain Res. 1062*, 74–85.
(93) Liu, K., Gui, B., Sun, Y., Shi, N., Gu, Z., Zhang, T., and Sun, X. (2013) Inhibition of L-type Ca2+ channels by curcumin requires a novel protein kinase-theta isoform in rat hippocampal neurons. *Cell Calcium 53*, 195–203.
(94) Belevych, A. E., Warrier, S., and Harvey, R. D. (2002) Genistein inhibits cardiac L-type Ca(2+) channel activity by a tyrosine kinase-independent mechanism. *Mol. Pharmacol. 62*, 554–565.
(95) Zhang, L. P., Yin, J. X., Liu, Z., Zhang, Y., Wang, Q. S., and Zhao, J. (2006) Effect of resveratrol on L-type calcium current in rat ventricular myocytes. *Acta Pharmacol. Sin. 27*, 179–183.
(96) Zhu, F. X., Zhang, X. Y., Olszewski, M. A., and Robinson, N. E. (1997) Mechanism of capsaicin-induced relaxation in equine tracheal smooth muscle. *Am. J. Physiol. 273*, L997–1001.
(97) Stumpff, F., Que, Y., Boxberger, M., Strauss, O., and Wiederholt, M. (1999) Stimulation of maxi-K channels in trabecular meshwork by tyrosine kinase inhibitors. *Invest. Ophthalmol. Vis. Sci. 40*, 1404–1417.
(98) Li, H. F., Chen, S. A., and Wu, S. N. (2000) Evidence for the stimulatory effect of resveratrol on Ca(2+)-activated K+ current in vascular endothelial cells. *Cardiovasc. Res. 45*, 1035–1045.

(99) Morin, D., Barthelemy, S., Zini, R., Labidalle, S., and Tillement, J. P. (2001) Curcumin induces the mitochondrial permeability transition pore mediated by membrane protein thiol oxidation. *FEBS Lett. 495*, 131–136.
(100) Ligeret, H., Barthelemy, S., Zini, R., Tillement, J. P., Labidalle, S., and Morin, D. (2004) Effects of curcumin and curcumin derivatives on mitochondrial permeability transition pore. *Free Radic. Biol. Med. 36*, 919–929.
(101) Yoon, H. S., Moon, S. C., Kim, N. D., Park, B. S., Jeong, M. H., and Yoo, Y. H. (2000) Genistein induces apoptosis of RPE-J cells by opening mitochondrial PTP. *Biochem. Biophys. Res. Commun. 276*, 151–156.
(102) Tian, X. M., and Zhang, Z. X. (2003) Resveratrol promote permeability transition pore opening mediated by Ca2+ (trn. chi.). *Yao Xue Xue Bao 38*, 81–84.
(103) Lorenz, M., Hellige, N., Rieder, P., Kinkel, H. T., Trimpert, C., Staudt, A., Felix, S. B., Baumann, G., Stangl, K., and Stangl, V. (2008) Positive inotropic effects of epigallocatechin-3-gallate (EGCG) involve activation of Na+/H+ and Na+/Ca2+ exchangers. *Eur. J. Heart Fail. 10*, 439–445.
(104) Feng, W., Hwang, H. S., Kryshtal, D. O., Yang, T., Padilla, I. T., Tiwary, A. K., Puschner, B., Pessah, I. N., and Knollmann, B. C. (2012) Coordinated Regulation of Murine Cardiomyocyte Contractility by Nanomolar (-)-Epigallocatechin-3-Gallate, the Major Green Tea Catechin. *Mol. Pharmacol. 82*, 993–1000.
(105) Nabekura, T., Kamiyama, S., and Kitagawa, S. (2005) Effects of dietary chemopreventive phytochemicals on P-glycoprotein function. *Biochem. Biophys. Res. Commun. 327*, 866–870.
(106) Okura, T., Ibe, M., Umegaki, K., Shinozuka, K., and Yamada, S. (2010) Effects of dietary ingredients on function and expression of P-glycoprotein in human intestinal epithelial cells. *Biol. Pharm. Bull. 33*, 255–259.
(107) Anuchapreeda, S., Leechanachai, P., Smith, M. M., Ambudkar, S. V., and Limtrakul, P. N. (2002) Modulation of P-glycoprotein expression and function by curcumin in multidrug-resistant human KB cells. *Biochem. Pharmacol. 64*, 573–582.
(108) Chearwae, W., Wu, C. P., Chu, H. Y., Lee, T. R., Ambudkar, S. V., and Limtrakul, P. (2006) Curcuminoids purified from turmeric powder modulate the function of human multidrug resistance protein 1 (ABCC1). *Cancer Chemother. Pharmacol. 57*, 376–388.
(109) Chearwae, W., Shukla, S., Limtrakul, P., and Ambudkar, S. V. (2006) Modulation of the function of the multidrug resistance-linked ATP-binding cassette transporter ABCG2 by the cancer chemopreventive agent curcumin. *Mol. Cancer Ther. 5*, 1995–2006.
(110) Zhu, Z., Wang, Y., Liu, Z., Wang, F., and Zhao, Q. (2012) Inhibitory effects of epigallocatechin-3-gallate on cell proliferation and the expression of HIF-1α and P-gp in the human pancreatic carcinoma cell line PANC-1. *Oncol. Rep. 27*, 1567–1572.
(111) Yang, X., Thomas, D. P., Zhang, X., Culver, B. W., Alexander, B. M., Murdoch, W. J., Rao, M. N., Tulis, D. A., Ren, J., and Sreejayan, N. (2006) Curcumin inhibits platelet-derived growth factor-stimulated vascular smooth muscle cell function and injury-induced neointima formation. *Arterioscler. Thromb. Vasc. Biol. 26*, 85–90.
(112) Little, P. J., Getachew, R., Rezaei, H. B., Sanchez-Guerrero, E., Khachigian, L. M., Wang, H., Liao, S., Zheng, W., Ballinger, M. L., and Osman, N. (2012) Genistein inhibits PDGF-stimulated proteoglycan synthesis in vascular smooth muscle without blocking PDGFβ receptor phosphorylation. *Arch. Biochem. Biophys. 525*, 25–31.
(113) Godichaud, S., Si-Tayeb, K., Auge, N., Desmouliere, A., Balabaud, C., Payrastre, B., Negre-Salvayre, A., and Rosenbaum, J. (2006) The grape-derived polyphenol resveratrol

differentially affects epidermal and platelet-derived growth factor signaling in human liver myofibroblasts. *Int. J. Biochem. Cell. Biol. 38*, 629–637.
(114) Mahmmoud, Y. A. (2008) Capsaicin stimulates uncoupled ATP hydrolysis by the sarcoplasmic reticulum calcium pump. *J. Biol. Chem. 283*, 21418–21426.
(115) Bilmen, J. G., Khan, S. Z., Javed, M. H., and Michelangeli, F. (2001) Inhibition of the SERCA Ca2+ pumps by curcumin. Curcumin putatively stabilizes the interaction between the nucleotide-binding and phosphorylation domains in the absence of ATP. *Eur. J. Biochem. 268*, 6318–6327.
(116) Kargacin, M. E., Emmett, T. L., and Kargacin, G. J. (2011) Epigallocatechin-3-gallate has dual, independent effects on the cardiac sarcoplasmic reticulum/endoplasmic reticulum Ca2+ ATPase. *J. Muscle. Res. Cell Motil. 32*, 89–98.
(117) Sulaiman, M., Matta, M. J., Sunderesan, N. R., Gupta, M. P., Periasamy, M., and Gupta, M. (2010) Resveratrol, an activator of SIRT1, upregulates sarcoplasmic calcium ATPase and improves cardiac function in diabetic cardiomyopathy. *Am. J. Physiol. Heart. Circ. Physiol. 298*, H833–H843.
(118) Wang, W., Lerea, K. M., Chan, M., and Giebisch, G. (2000) Protein tyrosine kinase regulates the number of renal secretory K channels. *Am. J. Physiol. Renal. Physiol. 278*, F165–171.
(119) Caterina, M. J., Schumacher, M. A., Tominaga, M., Rosen, T. A., Levine, J. D., and Julius, D. (1997) The capsaicin receptor: a heat-activated ion channel in the pain pathway. *Nature 389*, 816–824.
(120) Cao, E., Liao, M., Cheng, Y., and Julius, D. (2013) TRPV1 structures in distinct conformations reveal activation mechanisms. *Nature 504*, 113–118.
(121) Kuenzi, F. M., and Dale, N. (1996) Effect of capsaicin and analogues on potassium and calcium currents and vanilloid receptors in Xenopus embryo spinal neurones. *Br. J. Pharmacol. 119*, 81–90.
(122) Pingle, S. C., Matta, J. A., and Ahern, G. P. (2007) Capsaicin receptor: TRPV1 a promiscuous TRP channel. *Handb. Exp. Pharmacol.* 155–171.
(123) Martelli, L., Ragazzi, E., di Mario, F., Martelli, M., Castagliuolo, I., Dal Maschio, M., Palu, G., Maschietto, M., Scorzeto, M., Vassanelli, S., and Brun, P. (2007) A potential role for the vanilloid receptor TRPV1 in the therapeutic effect of curcumin in dinitrobenzene sulphonic acid-induced colitis in mice. *Neurogastroenterol. Motil. 19*, 668–674.
(124) Leamy, A. W., Shukla, P., McAlexander, M. A., Carr, M. J., and Ghatta, S. (2011) Curcumin ((E,E)-1,7-bis(4-hydroxy-3-methoxyphenyl)-1,6-heptadiene- 3,5-dione) activates and desensitizes the nociceptor ion channel TRPA1. *Neurosci. Lett. 503*, 157–162.
(125) Kurogi, M., Miyashita, M., Emoto, Y., Kubo, Y., and Saitoh, O. (2012) Green Tea Polyphenol Epigallocatechin Gallate Activates TRPA1 in an Intestinal Enteroendocrine Cell Line, STC-1. *Chemical. Senses 37*, 167–177.
(126) Wong, C. O., Huang, Y., and Yao, X. (2010) Genistein potentiates activity of the cation channel TRPC5 independently of tyrosine kinases. *Br. J. Pharmacol. 159*, 1486–1496.
(127) Yu, L., Wang, S., Kogure, Y., Yamamoto, S., Noguchi, K., and Dai, Y. (2013) Modulation of TRP channels by resveratrol and other stilbenoids. *Mol. Pain 9*, 3.
(128) Enyeart, J. A., Liu, H., and Enyeart, J. J. (2008) Curcumin inhibits bTREK-1 K+ channels and stimulates cortisol secretion from adrenocortical cells. *Biochem. Biophys. Res. Commun. 370*, 623–628.
(129) Patel, S. K., Jackson, L., Warren, A. Y., Arya, P., Shaw, R. W., and Khan, R. N. (2013) A

role for two-pore potassium (K2P) channels in endometrial epithelial function. *J. Cell. Mol. Med. 17*, 134–146.
(130) Gierten, J., Ficker, E., Bloehs, R., Schlömer, K., Kathöfer, S., Scholz, E., Zitron, E., Kiesecker, C., Bauer, A., Becker, R., Katus, H. A., Karle, C. A., and Thomas, D. (2008) Regulation of two-pore-domain (K2P) potassium leak channels by the tyrosine kinase inhibitor genistein. *Br. J. Pharmacol. 154*, 1680–1690.
(131) Chen, W. H., Chen, Y., and Cui, G. H. (2005) Effects of TNF-alpha and curcumin on the expression of VEGF in Raji and U937 cells and on angiogenesis in ECV304 cells. *Chin. Med. J. (Engl) 118*, 2052–2057.
(132) Lamy, S., Gingras, D., and Béliveau, R. (2002) Green tea catechins inhibit vascular endothelial growth factor receptor phosphorylation. *Cancer Res. 62*, 381–385.
(133) Dann, J. M., Sykes, P. H., Mason, D. R., and Evans, J. J. (2009) Regulation of Vascular Endothelial Growth Factor in endometrial tumour cells by resveratrol and EGCG. *Gynecol. Oncol. 113*, 374–378.
(134) Yu, X., Mi, M., and Zhu, J. (2008) Genistein Inhibits the Expression of Vascular Endothelial Growth Factor in MDA-MB-453 Breast Cancer Cells. *U. S. Chin. J. Lymphology Oncol. 7*, 8–13.
(135) Milesi, V., Rebolledo, A., Alvis, A. G., Raingo, J., and Grassi de Gende, A. O. (2001) Voltage-activated sodium current is inhibited by capsaicin in rat atrial myocytes. *Biochem. Biophys. Res. Commun. 282*, 965–970.
(136) Liu, L., Oortgiesen, M., Li, L., and Simon, S. A. (2001) Capsaicin inhibits activation of voltage-gated sodium currents in capsaicin-sensitive trigeminal ganglion neurons. *J. Neurophysiol. 85*, 745–758.
(137) Cao, X., Cao, X., Xie, H., Yang, R., Lei, G., Li, F., Li, A., Liu, C., and Liu, L. (2007) Effects of capsaicin on VGSCs in TRPV1−/− mice. *Brain Res. 1163*, 33–43.
(138) Kim, T. H., Lim, J.-M., Kim, S. S., Kim, J., Park, M., and Song, J.-H. (2009) Effects of (-) epigallocatechin-3-gallate on Na(+) currents in rat dorsal root ganglion neurons. *Eur. J. Pharmacol. 604*, 20–26.
(139) Paillart, C., Carlier, E., Guedin, D., Dargent, B., and Couraud, F. (1997) Direct block of voltage-sensitive sodium channels by genistein, a tyrosine kinase inhibitor. *J. Pharmacol. Exp. Ther. 280*, 521–526.
(140) Wallace, C. H. R., Baczko, I., Jones, L., Fercho, M., and Light, P. E. (2006) Inhibition of cardiac voltage-gated sodium channels by grape polyphenols. *Br. J. Pharmacol. 149*, 657–665.